Title:

Cell-Type-Specific Decrease of the Intrinsic Excitability of Motor Cortical Pyramidal Neurons in Parkinsonian Mice

Abbreviated title:

Intrinsic Adaptations of M1 Pyramidal Cells in PD

Authors: Liqiang Chen, Yerim Kim, Hong-Yuan Chu

Affiliation: Center for Neurodegenerative Science, Van Andel Institute

Address: 333 Bostwick Ave, N.E., Grand Rapids, MI 49503

Correspondence: Hong-Yuan Chu, Ph.D., email: hongyuan.chu@vai.org

Conflict of interest: The authors declare no competing financial interests.

Acknowledgements: This work was supported by fund from Van Andel Institute (H.Y.C). The authors thank Mr. David Nadziejka for technical editing.

Abstract

The hypokinetic motor symptoms of Parkinson's disease (PD) are closely linked with a decreased motor cortical output as a consequence of elevated basal ganglia inhibition. However, whether and how the loss of dopamine alters the cellular properties of motor cortical neurons in PD remains undefined. We induced experimental parkinsonism in adult C57BL6 mice of both sexes by injecting neurotoxin, 6-hydroxydopamine, into the medial forebrain bundle. By using *ex vivo* patch-clamp recording and retrograde tracing approach, we found that the intrinsic excitability of pyramidal tract neurons (PTNs) in the motor cortical layer 5b was greatly decreased following the degeneration of midbrain dopaminergic neurons; but the intratelencephalic neurons (ITNs) were not affected. The cell-type-specific intrinsic adaptations were associated with a significant broadening of the action potentials in PTNs but not in ITNs. Moreover, the loss of midbrain dopaminergic neurons impaired the capability of M1 PTNs to sustain high-frequency firing, which could underlie their abnormal pattern of activity in the parkinsonian state. We also showed that the decreased excitability and broadened action potentials were largely caused by a disrupted function of the large conductance, Ca^{2+}-activated K^{+} channels. The restoration of dopaminergic neuromodulation failed to rescue the impaired intrinsic excitability of M1 PTNs in parkinsonian mice. Altogether, our data show cell-type-specific decreases of the excitability of M1 pyramidal neurons following the loss of midbrain dopaminergic neurons. Thus, intrinsic adaptations in the motor cortex, together with pathological basal ganglia inhibition, underlie the decreased motor cortical output in parkinsonian state and exacerbate parkinsonian motor deficits.

37 **Significance statement**

38 The degeneration of midbrain dopaminergic neurons in Parkinson's disease remodels
39 the connectivity and function of cortico–basal ganglia–thalamocortical network.
40 However, whether and how the loss of dopamine and aberrant basal ganglia activity
41 alter motor cortical circuitry remain undefined. We found that pyramidal neurons in the
42 layer 5b of the primary motor cortex (M1) exhibit distinct adaptations in response to the
43 loss of midbrain dopaminergic neurons, depending on their long-range projections.
44 Besides the decreased thalamocortical synaptic excitation as proposed by the classical
45 model of Parkinson's pathophysiology, these results, for the first time, show novel
46 cellular and molecular mechanisms underlying the abnormal motor cortical output in
47 parkinsonian state.

48

Introduction

The degeneration of dopamine (DA) neurons in the substantia nigra (SN) alters the connection and computation of cortico–basal ganglia–thalamocortical network, which underlies the devastating motor symptoms in Parkinson's disease (PD), including akinesia, bradykinesia, and rigidity (Albin et al., 1989; Galvan and Wichmann, 2008; McGregor and Nelson, 2019). Specially, the loss of SN DA neurons increases and decreases the activities of indirect and direct pathways, respectively, which disrupts the balanced activity between striatal direct and indirect pathways, leading to the hypokinetic symptoms in PD (Albin et al., 1989; DeLong, 1990). The pathway-specific alterations in the striatum following the loss of SN DA neurons induce numerous cellular and synaptic changes in the basal ganglia nuclei and extended brain regions, which further drive the abnormal neural activity throughout the cortico–basal ganglia–thalamocortical network in experimental parkinsonism (Gittis et al., 2011; Kita and Kita, 2011; Fieblinger et al., 2014; Chu et al., 2015, 2017; Mathai et al., 2015; Shen et al., 2015; Parker et al., 2016, 2018; Sharott et al., 2017; McIver et al., 2019; Willard et al., 2019).

The primary motor cortex (M1) plays essential and complex roles in motor control and motor learning and is a key node in the cortico–basal ganglia–thalamocortical network (Shepherd, 2013; Ebbesen and Brecht, 2017; Ebbesen et al., 2018). M1 is a laminar structure and contains a heterogeneous group of neurons that differ in gene expression, morphology, connectivity, and electrophysiological properties (Sheets et al., 2011; Oswald et al., 2013; Shepherd, 2013; Suter et al., 2013; Economo et al., 2018). These neurons can be classified into the intratelencephalic neurons (ITNs) distributed

72 across the layers (L) 2-6 and the pyramidal tract neurons (PTNs) that mainly locate
73 within the L5b (Oswald et al., 2013; Shepherd, 2013). Both PTNs and ITNs project to
74 the striatum and receive basal ganglia feedbacks through the transition of the motor
75 thalamus (Bodor et al., 2008; Kita and Kita, 2011; Kress et al., 2013; Lee et al., 2020).
76 In physiological state, M1 network dynamics plays an essential role in the execution and
77 coordination of complex movements and the acquisition of motor skills (Guo et al.,
78 2015a; Kawai et al., 2015; Sreenivasan et al., 2016; Barthas and Kwan, 2017; Ebbesen
79 et al., 2017; Wang et al., 2017; Economo et al., 2018; Sauerbrei et al., 2020). In
80 parkinsonian state, M1 exhibits an aberrant oscillation and bursting pattern of activity at
81 both individual neuron and population levels (Goldberg et al., 2002; Mallet et al., 2008;
82 Pasquereau and Turner, 2011; Shimamoto et al., 2013; Hemptinne et al., 2015;
83 Pasquereau et al., 2016), which disrupt its normal function in motor control and motor
84 learning.
85 The abnormal neuronal activity in the M1 has been hypothesized to a
86 consequence of pathological basal ganglia output (Hosp et al., 2011, 2015; Pasquereau
87 and Turner, 2011; Guo et al., 2015b; Pasquereau et al., 2016), but the cellular
88 adaptations could also play a key role in such abnormal activities. Moreover, compelling
89 evidence suggests that PTNs and ITNs may adapt differently to the degeneration of
90 midbrain DA neurons (Pasquereau and Turner, 2011; Pasquereau et al., 2016).Thus,
91 we hypothesized that loss of SN DA neurons alters the intrinsic properties of M1
92 pyramidal neurons in a cell-type-specific manner, and that the intrinsic adaptations
93 contribute to the abnormal neuronal activity of M1 in parkinsonian state. We addressed

these hypotheses using electrophysiology and retrograde tracing approach in mice with 6-hydroxydopmaine (6-OHDA) lesion, an established model of parkinsonism.

Material and Methods

Animals

Mice were housed up to four animals per cage under a 12-h light/12-h dark cycle with access to food and water *ad libitum* in accordance with Van Andel Institute IACUC and NIH guidelines for care and use of animals.

Stereotaxic surgery

Mice were deeply anesthetized under 2% isoflurane, were placed in a stereotaxic frame (Kopf), and were supported by a thermostatic heating pad. To induce degeneration of SN DA neurons, 6-OHDA (3-4 mg/mL, 1.0 μL) was injected unilaterally into the medial forebrain bundle (MFB, from bregma (in mm): AP, -0.7, ML, +1.2, DV, -4.7) over 10 min using a 10-μl syringe (Hamilton) and a motorized microinjector (Stoelting, Wood Dale, IL, USA) (Chu et al., 2017). Controls were injected in the same location with vehicle. Desipramine (25 mg/kg) and pargyline (50 mg/kg) were subcutaneously injected 30-40 min prior to 6-OHDA injection, to enhance the sensitivity and toxicity of 6-OHDA (Chu et al., 2015, 2017). To label and identify PTNs and ITNs in the M1, animals also received red or green Retrobeads (0.3 μL, Lumafluor, Inc) injected into the ipsilateral pontine nuclei (from bregma (in mm): AP, -5.0; ML, +0.6; DV, -5.0; 0.3 μl per injection) or the contralateral dorsolateral striatum (from bregma (in mm): AP, +0.4; ML, -2.0; DV, -2.8). The surgical wound was closed using sutures and mice were allowed to recover after

117 surgery in a heated cage with access to food and water at the cage-floor level. Motor
118 cortex slices containing the forelimb regions from 6-OHDA- or vehicle-injected mice
119 were prepared 3-4 weeks after surgery for *ex vivo* electrophysiology (days post-surgery:
120 control = 27 [22, 28] days, n = 19 mice; 6-OHDA = 24 [22, 27] days, n = 19 mice).
121

122 **Slice preparation**

123 Mice were deeply anesthetized with intraperitoneal avertin (250 mg/kg) and then were
124 perfused transcardially with ice-cold, sucrose-based, artificial cerebrospinal fluid (aCSF)
125 containing (in mM) 230 sucrose, 26 $NaHCO_3$, 10 glucose, 10 $MgSO_4$, 2.5 KCl, 1.25
126 NaH_2PO_4, and 0.5 $CaCl_2$. Next, coronal brain slices (250 μm) containing M1 forelimb
127 regions were prepared in the same slicing solution using a vibratome (VT1200S; Leica
128 Microsystems Inc., Buffalo Grove, IL, USA). Brain slices were kept in normal aCSF (in
129 mM: 126 NaCl, 26 $NaHCO_3$, 10 glucose, 2.5 KCl, 2 $CaCl_2$, 2 $MgSO_4$, 1.25 NaH_2PO_4, 1
130 sodium pyruvate and 0.005 L-glutathione) equilibrated with 95% O_2 and 5% CO_2 for 30
131 min at 35 °C and then held at room temperature until electrophysiological recording.
132

133 ***Ex vivo* electrophysiology recording**

134 Brain slices were transferred into a recording chamber perfused at a rate of 4 mL/min
135 with synthetic interstitial fluid (in mM: 126 NaCl, 26 $NaHCO_3$, 10 glucose, 3 KCl, 1.6
136 $CaCl_2$, 1.5 $MgSO_4$, 1.25 NaH_2PO_4) equilibrated with 95% O_2 and 5% CO_2 at 35 °C via a
137 feedback-controlled in-line heater (TC-324C, Warner Instruments). DNQX (20 μM), D-
138 APV (50 μM), and SR-95531 (10 μM) were routinely added to block synaptic
139 transmission mediated by ionotropic glutamatergic and GABAergic receptors. Neurons

140 were visualized and recorded under gradient contrast SliceScope 6000 (Scientifica, UK)
141 with infrared illumination using a CCD camera (SciCam Pro, Scientifica, UK) and
142 motorized micromanipulators (Scientifica, UK). Individual neurons labeled with
143 Retrobeads in the M1 L5b were identified using a 60X water immersion objective lens
144 (Olympus, Japan) and targeted for whole-cell patch-clamp recording, using a
145 MultiClamp 700B amplifier and a Digidata 1500B digitizer under the control of
146 pClamp11 (Molecular Devices, San Jose, USA). Data were collected at a sampling rate
147 of 20-50 KHz. Borosilicate glass pipettes for patch clamp recordings (4-7 MΩ) were
148 pulled using a micropipette puller (P1000, Sutter Instruments). Pipette capacitance was
149 compensated for before the formation of the whole-cell configuration. Series resistance
150 (Rs) was regularly monitored and compensated for with the bridge balance circuit in
151 current clamp mode. Liquid junction potential (about 11 mV) was corrected.
152 Retrobeads-labeled neurons in the L5b of M1 were recorded in whole-cell
153 current-clamp mode to study their intrinsic properties. In these experiments, glass
154 pipettes were filled with a potassium gluconate–based internal solution of (in mM) 140
155 K-gluconate, 3.8 NaCl, 1 $MgCl_2$, 10 HEPES, 0.1 Na_4-EGTA, 2 ATP-Mg, and 0.1 GTP-
156 Na, pH 7.3, osmolarity 290 mOsm. The resting membrane potential (V_m) was recorded
157 once the whole-cell configuration was obtained. The intrinsic properties and excitability
158 of M1 pyramidal neuron subtypes were studied by injecting a family of current steps
159 ranging from -80 pA to 720 pA in 40-pA increments and with a duration of 1 s. Current
160 injections were from V_m. Input resistance was determined by measuring the steady-
161 state voltage responses to a series of 1-s hyperpolarizing currents.

162 The rheobase, as an indicator of neuronal excitability, was defined as the current
163 intensity to elicit an action potential (AP) during a 1-s current injection. AP waveforms at
164 the rheobase were systematically analyzed and quantified. Specifically, the threshold of
165 AP was determined as the voltage level at which d*V*/d*t* exceeded 20 mV/ms. AP
166 amplitude was defined as the voltage difference between the threshold and the peak
167 voltage. AP half-width was measured as the time difference at 50% of AP amplitude.
168 Fast and medium afterhyperpolarizations (fAHPs and mAHPs) were measured as the
169 negative voltage peaks relative to the threshold within 2-5 ms and 20-50 ms from AP
170 threshold, respectively (Villalobos et al., 2004; Bean, 2007). To quantify spike trains,
171 spike frequency adaptation was measured as the ratio between the last inter-spike-
172 interval and the average of the first two inter-spike-intervals. The gain of the spike-
173 current curve was defined as the slope of the instantaneous spike-current curve.
174
175 **Immunohistochemistry**
176 Striatal immunoreactivity of tyrosine hydroxylase (TH) was assessed to validate the
177 degeneration of the nigrostriatal DA projections in vehicle- and 6-OHDA-injected mice.
178 Briefly, brain tissues were first fixed in 4% paraformaldehyde in 0.1 M phosphate buffer,
179 pH7.4, at 4 °C for 12 hours before rinsing in phosphate-buffered saline (PBS, 0.05 M;
180 pH 7.4). Tissues was re-sectioned at 70 μm using a vibratome (Leica VT1000S;
181 Microsystems Inc.). Immunochemical detection of TH was conducted in PBS containing
182 0.2% Triton X-100 (Fisher Scientific) and 2% normal donkey serum (Sigma-Aldrich, St.
183 Louis, MO). Brain sections were incubated in primary antibody (mouse anti-TH, 1:1000,
184 cat#: MAB318, Sigma-Aldrich, St. Louis, MO, USA) for 48 h at 4 °C or overnight at room

temperature (RT), washed in PBS, and then incubated in the secondary antibody (donkey anti-mouse Alexa Fluor 488, cat#: 715-545-150 or donkey anti-mouse Alexa Fluor 594, cat#715-585-150; 1: 500, Jackson ImmunoReseach) for 90 minutes at RT before washing with PBS. Brain sections were mounted on glass slides using VECTASHIELD antifade mounting medium (cat#: H-1000, Vector Laboratories, Burlingame, CA, USA) and were cover-slipped. TH immunoreactivity was imaged using an Olympus BX63F microscope equipped with an Olympus DP80 camera or a confocal laser scanning microscope (A1R; Nikon, Melville, USA). The intensity of TH immunofluorescence was quantified using ImageJ (NIH). All the mice with 6-OHDA injection showed > 80% TH immunoreactivity loss in the ipsilateral dorsal striatum versus contralateral dorsal striatum.

Experimental design and statistical analysis

Nineteen male and 19 female adult (4-5 months old) C57BL/6 mice were used in the study. Data were analyzed in Clampfit (Molecular Devices) and ImageJ (NIH). Statistics were done using Prism8 (GraphPad Software, San Diego, CA, USA). To minimize the assumption of the data normality, we used non-parametric, distribution-independent Mann-Whiney U (MWU) or Wilcoxon signed rank (WSR) tests for paired or non-paired data comparisons, respectively. The Holm-Bonferroni correction was applied for multiple comparisons. All tests were two-tailed, and an α-level of 0.05 was used to determine statistical significance. Results are reported as median and interquartile range. Boxplots illustrate the median (central line), interquartile range (box), and 10-90% range (whiskers) of data. Data are available upon request.

209 **Results**

210 **Cell-type-specific decrease in the intrinsic excitability of M1 L5b pyramidal**
211 **neurons following the loss of midbrain DA neurons.**

212 We compared the intrinsic excitability of projection-defined pyramidal neurons in the L5b
213 of M1 from vehicle-injected controls (hereinafter, “controls”) and from mice with 6-OHDA
214 lesion (hereinafter, “6-OHDA mice”). To distinguish M1 pyramidal neurons based on
215 long-range projections, Retrobeads were stereotaxically injected into the ipsilateral
216 pontine nuclei (Fig. 1A) and the contralateral striatum (Fig. 2A) to retrogradely label
217 PTNs (Fig. 1B) and ITNs (Fig. 2B), respectively. The intrinsic electrophysiological
218 properties of M1 PTNs and ITNs were assessed using whole-cell current-clamp
219 recording in the presence of antagonists of ionotropic glutamatergic and GABAergic
220 receptors, including DNQX (20 μM), D-APV (50 μM), and SR95531 (10 μM). All
221 recordings were conducted between 3 and 4 weeks post-surgery, when the level of
222 midbrain DA degeneration and functional adaptations in the brain have reached
223 maximum and been stabilized (Vila et al., 2000; Viaro et al., 2011). The data are
224 reported as median and interquartile range in the text and figures.

225 The intrinsic excitability of M1 pyramidal neuron subtypes was assessed by
226 somatic injection of a range of depolarizing currents in controls and 6-OHDA mice
227 (Figures 1C, D). We found that the gain of spike-current curve (control = 78.2 [67.4,
228 91.25] spikes/nA, n = 25 neurons/5 mice; 6-OHDA = 52.0 [44.7, 72.2] spikes/nA, n = 25
229 neurons/4 mice; p = 0.0015, MWU; Figures 1E) was significantly decreased in M1 PTNs
230 from 6-OHDA mice relative to those from controls. The same reduction was also
231 detected for the spike frequency (e.g. frequency at 720 pA current injection, control = 55

232 [47, 59] Hz, n = 25 neurons/5 mice; 6-OHDA = 38 [29, 53] Hz, n = 25 neurons/4 mice; p
233 = 0.0016, MWU; Figure 1F). M1 PTNs could sustain persistent firing with minimal spike
234 adaptation during repetitive firing in the physiological state (Figure 1C) (Oswald et al.,
235 2013; Suter et al., 2013). However, following the loss of midbrain DA neurons, PTNs
236 showed significantly enhanced spike adaptation. For instance, the spike adaptation of a
237 10- to15-Hz spike train, control = 1.06 [0.97, 1.26], n = 25 neurons/5 mice; 6-OHDA =
238 1.38 [1.17, 1.60], n = 25 neurons/4 mice; p = 0.0001, MWU (Figures 1C, G). These
239 results suggest a significant reduction in the intrinsic excitability of M1 PTNs following
240 the loss of midbrain DA neurons.

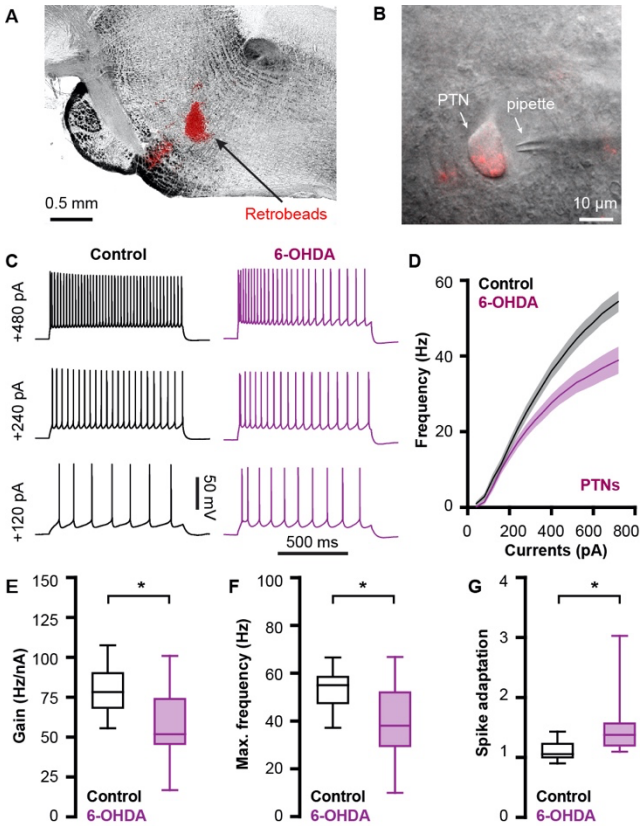

Figure 1. Decreased intrinsic excitability of PTNs in the L5b of M1 following the loss of midbrain DA neurons. A and B) Representative graphs showing the injection site of red Retrobeads in the pontine nuclei (**A**) and a retrogradely labeled PTN in L5b of M1 (**B**). **C and D**) Representative spike trains of PTNs evoked by somatic current injections from controls and 6-OHDA mice (**C**), and the frequency-current relationship of the PTNs from controls and 6-OHDA mice (**D**). **E-G**) Summarized results showing a reduced gain of spike-current curve (**E**), a decreased firing frequency in response to maximal current injections (i.e., 720 pA) (**F**), and an enhanced spike adaptations (**G**) in PTNs from 6-OHDA mice relative to those from controls. *, p < 0.05, MWU.

241

242 In contrast, M1 ITNs showed comparable spike-current relationships between the
243 controls and 6-OHDA mice. This was reflected by three measures, namely, a) the

244 unaltered gain of spike-current curve (control = 78 [54, 93] spikes/nA, n = 38 neurons/6
245 mice; 6-OHDA = 77 [67, 88] spikes/nA, n= 35 neurons/6 mice; p = 0.94, MWU; Figure
246 2D, E); b) the spike frequency at maximal (720 pA) current injection (control = 53 [38,
247 64] Hz, n = 38 neurons/6 mice; 6-OHDA = 50 [40, 58] Hz, n = 35 neurons/6 mice; p =
248 0.4, MWU; Figure 2D, F); and c) spike adaptations (control = 1.36 [1.08, 1.67], n= 38
249 neurons/6 mice; 6-OHDA = 1.20 [1.02, 1.61], n = 35 neurons/6 mice; p = 0.24, MWU;
250 Figure 2C, G). Altogether, our results thus suggest that the intrinsic excitability of PTNs,
251 but not ITNs, was significantly decreased following the loss of midbrain DA neurons,
252 that is, the M1 L5b pyramidal neurons exhibited cell-type-specific adaptations in their
253 intrinsic excitability in the parkinsonian state.

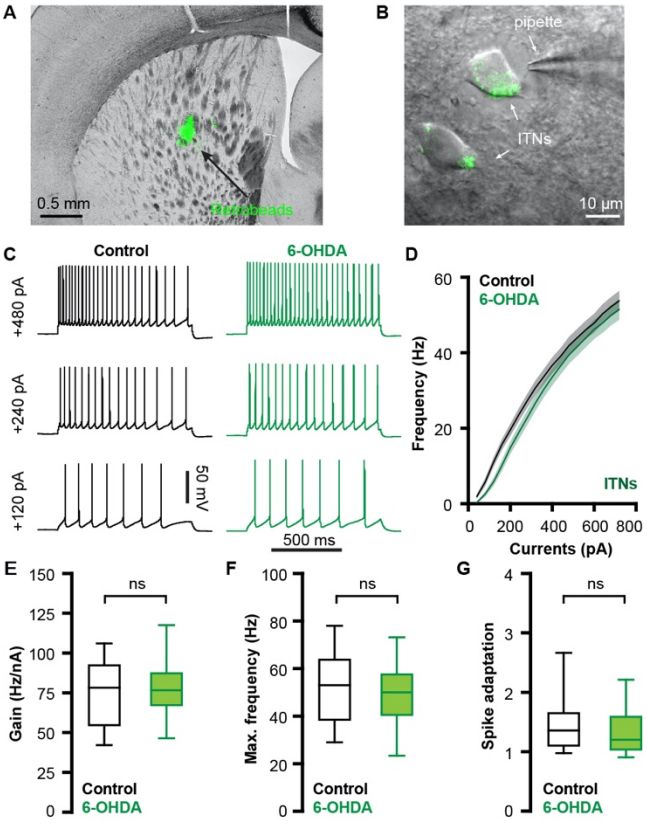

Figure 2. Intact intrinsic excitability of ITNs in the M1 L5b following the loss of midbrain DA neurons. A and B) Representative graphs showing the injection site of green Retrobeads in the dorsal striatum (**A**) and retrogradely labeled M1 L5b ITNs (**B**). **C and D**) Representative spikes trains evoked by somatic current injections into ITNs from control and 6-OHDA mice (**C**), and the frequency-current relationship of ITNs from controls and 6-OHDA mice (**D**). **E-G**) Boxplots showing an unaltered gain of spike-current curve (**E**), firing frequency in response to maximal current injections (i.e., 720 pA) (**F**), and spike adaptation (**G**) between ITNs from 6-OHDA mice and controls. ns, not significant, MWU.

254

255

Cell-type-specific changes in the passive membrane properties of M1 L5b pyramidal neurons following the loss of midbrain DA neurons.

In the absence of significant synaptic inputs, PTNs in 6-OHDA mice and controls had similar resting membrane potentials (V_m, control = -79.3 [-81.6, -77.9] mV, n = 25 neurons/5 mice; 6-OHDA = -79.7 [-81.5, -78.4] mV, n=25 neurons/4 mice; p = 0.85, MWU, Figure 3A). However, PTNs from 6-OHDA mice had an increased input resistance (R_m, control = 69.3 [60.1, 81.5] MΩ, n = 25 neurons/5 mice; 6-OHDA = 109.6 [73.0, 136.4] MΩ, n= 25 neurons/4 mice; p = 0.0028, MWU; Figures 3A, B). In contrast, ITNs showed a hyperpolarized V_m in 6-OHDA mice (control = -77.7 [-80.2, -75.0] mV, n=38 neurons/6 mice; 6-OHDA = -79.6 [-82.1, -77.2] mV, n = 35 neurons/6 mice; p = 0.012, MWU; Figure 3D). ITNs in 6-OHDA mice also had an unaltered R_m (control = 89.7 [60.4, 121.3] MΩ, n = 38 neurons/6 mice; 6-OHDA = 70.9 [54.7, 93] MΩ, n = 35 neurons/6 mice; p = 0.067, MWU; Figure 3E). Changes in V_m and R_m were associated with a significant increase in rheobase in ITNs (control= 80.8 [51.3, 125] pA, n = 36 neurons/6 mice; 6-OHDA = 125 [86, 191] pA, n = 35 neurons/6 mice; p = 0.002, MWU; Figure 3F). PTNs had unaltered rheobase following the loss of midbrain DA neurons (control = 82 [47, 163] pA, n= 25 neurons/5 mice; 6-OHDA = 79 [56, 120] pA, n = 25 neurons/4 mice; p = 0.645, MWU; Figure 3C). Thus, the loss of midbrain DA neurons induced distinct adaptations in passive membrane properties of PTNs and ITNs in M1.

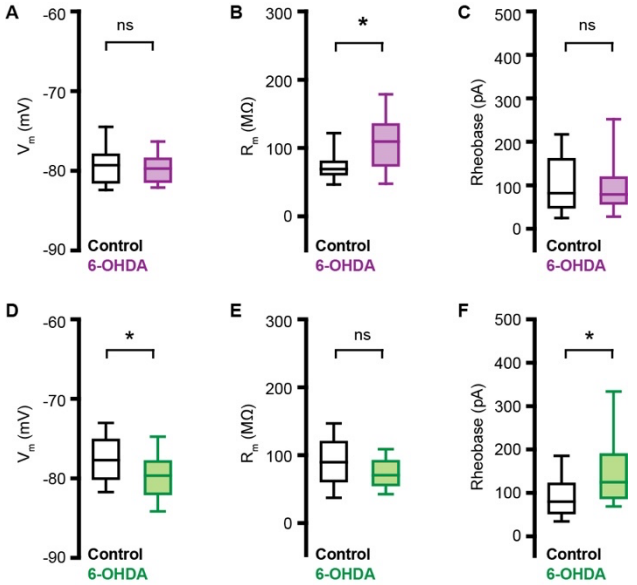

Figure 3. Distinct changes in the passive membrane properties of PTNs and ITNs in the M1 L5b following the loss of midbrain DA neurons. A-C) Boxplots showing changes in the resting membrane potential (**A**), input resistance (**B**), and rheobase (**C**) of PTNs from 6-OHDA mice relative to those from controls. **D-F**) Boxplots showing changes in in the resting membrane potential (**D**), input resistance (**E**), and rheobase (**F**) of ITNs from 6-OHDA mice relative to those from controls. ns, not significant; *, $p < 0.05$, MWU.

Cell-type-specific changes in action potential waveforms of M1 L5b pyramidal neurons following the loss of midbrain DA neurons.

The shape of the action potential is determined by the interaction of numerous voltage-gated ion channels and has profound effects on firing rate and pattern of neurons (Bean, 2007). We therefore analyzed the morphology of AP waveforms of PTNs (Figure 4A) and ITNs (Figures 4G) from controls and 6-OHDA mice. Following the loss of the midbrain DA neurons, M1 PTNs showed a striking AP broadening (AP half-width, controls = 0.69 [0.62, 0.75] ms, n = 25 neurons/5 mice; 6-OHDA = 0.85 [0.68, 1.23] ms, n = 25 neurons/4 mice; p = 0.005, MWU; Figure 4B). The broadened AP of PTNs was associated with a significantly prolonged AP rise time (controls = 0.22 [0.19, 0.24] ms, n = 25 neurons/5 mice; 6-OHDA = 0.25 [0.22, 0.32] ms, n = 25 neurons/4 mice; p < 0.002, MWU; Figures 4C) and also a prolonged decay time (controls = 0.60 [0.53, 0.68] ms, n = 25 neurons/5 mice, 6-OHDA = 0.80 [0.58, 1.3] ms, 25 neurons/4 mice; p = 0.0035, MWU; Figure 4D). Further, the maximal rates of AP depolarization and repolarization of M1 PTNs also greatly decreased. The maximal AP rise rate in controls = 358 [306, 437]

mV/ms, n = 25 neurons/5 mice, while the maximal AP rise rate in 6-OHDA mice = 295 [245, 339] mV/ms, n= 25 neurons/4 mice; p = 0.0008, MWU (Figure 4E). The maximal AP decay rate, controls = -112 [-104, -130] mV/ms, n = 25 neurons/5 mice, and 6-OHDA = -84 [-64, -106] mV/ms, n = 25 neurons/4 mice; p = 0.0001, MWU (Figure 4F). Thus, the decreased excitability of PTNs is largely caused by an abnormal AP broadening, involving impaired AP depolarization and repolarization.

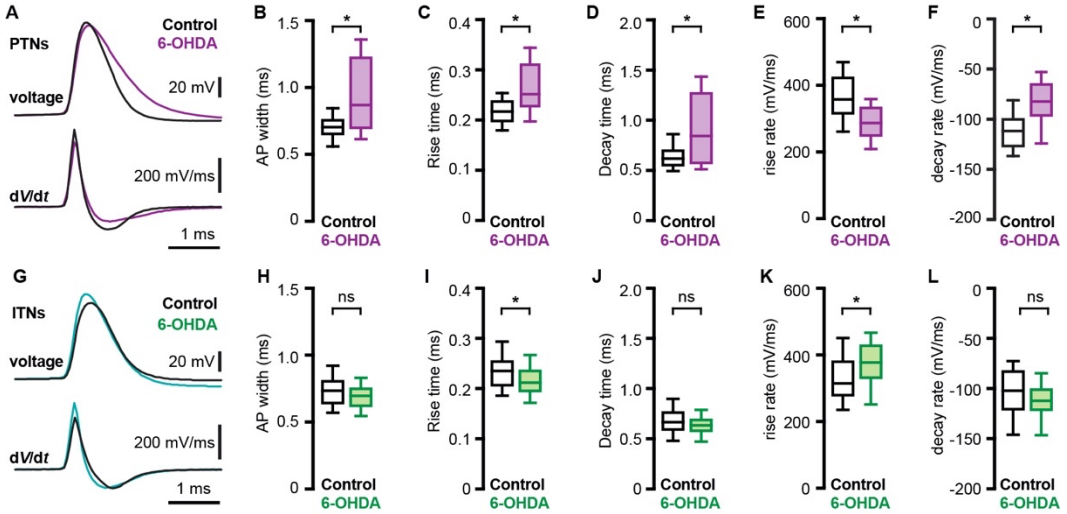

Figure 4. Distinct changes in AP waveforms of PTNs and ITNs in the M1 L5b following loss of midbrain DA neurons. A) **Top**, representative AP waveforms of PTNs from controls and 6-OHDA mice. APs were aligned at threshold and overlaid for comparison. **Bottom**, the corresponding *d*V/*d*t traces plotted against time, showing depolarizing and repolarizing rates of APs. **B**) Boxplot showing broadened AP width in PTNs from 6-OHDA mice relative to those from controls. **C and D**), Boxplots showing prolonged AP rise time (**C**) and decay time (**D**) in PTNs from 6-OHDA mice relative to those from controls. **E and F**), Boxplots showing decreased AP rise rate (**E**) and decay rate (**F**) in PTNs from 6-OHDA mice relative to those from controls. **G**) **Top**, representative AP waveforms of ITNs from controls and 6-OHDA mice. APs were aligned at threshold and overlaid for comparison. **Bottom**, the corresponding *d*V/*d*t traces plotted against time, showing depolarizing and repolarizing rates of APs. **H**) Boxplot showing similar AP width in ITNs from 6-OHDA mice relative to those from controls. **I-J**) Boxplots showing a shorter AP rise time (**I**) but similar decay time (**J**) in ITNs from 6-OHDA mice relative to those from controls. **K-L**) Boxplots showing an increased AP rise rate (**K**) but similar decay rate (**L**) in ITNs from 6-OHDA mice relative to those from controls. ns, not significant; *, p < 0.05, MWU.

In contrast, ITNs from controls and 6-OHDA mice showed similar AP width (control = 0.73 [0.64, 0.81] ms; n = 38 neurons/6 mice, 6-OHDA = 0.70 [0.61, 0.75] ms, n = 36 neurons/6 mice; p = 0.2, MWU; Figure 4H). The similar AP width of ITNs was

301 associated with an unaltered decay time and decay rate. The decay time for controls =
302 0.67 [0.58, 0.77] ms, n = 38 neurons/6 mice, while for 6-OHDA = 0.63 [0.57, 0.70] ms, n
303 = 35 neurons/6 mice; p = 0.15, MWU (Figure 4J). The decay rate values were, for
304 controls = -102 [-82, -122] mV/ms, n = 38 neurons/6 mice, and for 6-OHDA = -112 [-
305 100, -122] mV/ms, n = 35 neurons/6 mice; p = 0.1, MWU (Figure 4L). Moreover, ITNs
306 from 6-OHDA mice exhibited a faster AP depolarization relative to those from controls,
307 as reflected by a shorter rise time (controls = 0.24 [0.21, 0.26) ms, n = 38 neurons/6
308 mice; 6-OHDA = 0.21 [0.19, 0.24] ms, n = 35 neurons/6 mice; p = 0.03, MWU; Figure 4I]
309 and also a faster rise rate (control = 314 [276, 383] mV/ms, n = 38 neurons/6 mice; 6-
310 OHDA = 377 [329, 431] mV/ms, n = 35 neurons/6 mice; p = 0.009, MWU; Figure 4K).
311 Thus, these results suggest that ITNs of 6-OHDA mice had subtler changes in AP
312 waveforms and that efficient AP depolarization is likely a compensatory mechanism for
313 the hyperpolarized V_m and reduced R_m (Figures 3D, E), leading to an unaltered
314 superathreshold excitability (Figures 2C, D).
315

316 **Progressive alterations in AP waveforms of PTNs during repetitive firing**
317 **following the loss of SN DA neurons.**

318 In the physiological state, the burst pattern of activity of M1 PTNs is closely linked to
319 movement parameters, but this specificity of movement encoding is disrupted in PD
320 (Pasquereau et al., 2016; Economo et al., 2018; Sauerbrei et al., 2020). In addition,
321 PTNs show a decreased intraburst firing rate in MPTP-treated animals (Pasquereau
322 and Turner, 2011). We predicted that the altered intrinsic properties of PTNs contribute
323 to these *in vivo* observations in the parkinsonian state. Thus, spike trains containing 10-

15 spikes were elicited from M1 PTNs in controls and 6-OHDA mice, and the waveform of the first and the last APs within a spike train were analyzed to study progressive changes during repetitive firing.

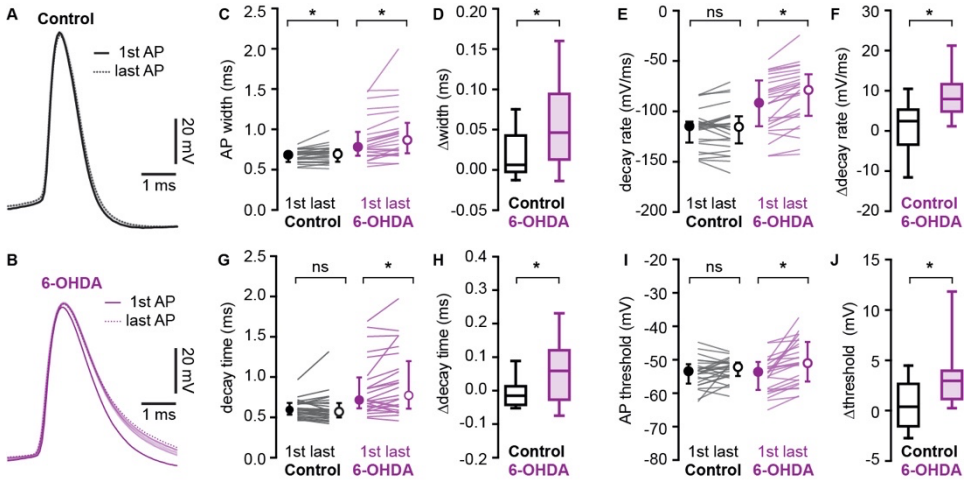

Figure 5. Progressive changes in AP waveforms of M1 PTNs during repetitive firing. **A-B**) APs from a 10- to15-Hz spike train were superimposed for PTNs from control (**A**) or 6-OHDA mice (**B**). APs were aligned at threshold, and the solid and dashed lines indicated the first and the last APs from the spike train, respectively. All the other APs were shown as transparent lines. **C-D**) Summarized graphs showing the alterations of AP width between the first and the last APs. Each line in (**C**) connects the AP width of the first and the last APs from the same spike train. Filled and open circles indicate the median plus interquartile range of the first and the last AP width of PTNs, respectively. (**D**) Boxplots showing the AP width difference between the first and the last APs was greater in PTNs from 6-OHDA mice relative to those from controls. **E-F**) Summarized graphs showing alterations of AP decay rate between the first and the last APs (**E**) and greater changes of AP decay rate in PTNs from 6-OHDA mice relative to those from controls (**F**). **G-H**) Summarized graphs showing alterations of AP decay time between the first and the last APs (**G**), and greater changes of AP decay time in PTNs from 6-OHDA mice relative to those from controls (**H**). **I-J**) Summarized graphs showing alterations of AP threshold between the first and the last APs (**I**), and greater changes of AP threshold in PTNs from 6-OHDA mice relative to those from controls (**J**). ns, not significant; *, $p < 0.05$, WSR.

The literature suggests that M1 PTNs have the capacity for high-frequency AP firing (300-450 Hz) (Suter et al., 2013). We also noted constant AP waveforms during repetitive firing in the control mice (Fig. 5A). Specifically, the PTNs from control mice showed subtle AP broadening during repetitive firing (AP width in controls, the first AP = 0.68 [0.60, 0.72] ms, the last AP = 0.69 [0.60, 0.75] ms, n = 25 neurons/5 mice; p = 0.013, WSR; Figure 5C). They also showed an unaltered decay rate (the first AP = -114 [-110, -131] mV/ms, the last AP = -115 [-105, -132] mV/ms, n = 25 neurons/5 mice; p =

335 0.57, WSR; Figure 5E) and an unaltered decay time (the first AP = 0.59 [0.53, 0.68] ms,
336 the last AP = 0.57 [0.50, 0.68] ms, n = 25 neurons/5 mice; p = 0.26, WSR; Figure 5G)
337 between the first and the last APs during repetitive firing. In addition, the AP threshold of
338 M1 PTNs from controls was also constant between the first and the last AP (threshold,
339 the first AP = -53.5 [-57.2, -51.4] mV, and the last AP = -52.3 [-54.9, -50.9] mV; n = 25
340 neurons/5 mice; p = 0.26, WSR; Figure 5I). The constant AP parameters of PTNs during
341 repetitive firings are key to delivering motor commands to subcortical premotor centers
342 with temporal precision during movement initiation and execution.

343 In contrast, PTNs from 6-OHDA mice showed progressive AP broadening during
344 repetitive firing (the first AP width = 0.78 [0.67, 0.97] ms, the last AP = 0.88 [0.70, 1.08]
345 ms, n = 25 neurons/4 mice; p = 0.0001, WSR; Figure 5C). This AP broadening was
346 associated with a significantly decreased AP decay rate (the first AP = -91.6 [-69.3, -
347 114.7] mV/ms, the last AP = -78.7 [-63.2, -104.4] mV/ms, n = 25 neurons/4 mice; p =
348 0.0001, WSR; Figure 5E) and decay time (the first AP = 0.72 [0.61, 1.0] ms, the last AP
349 = 0.77 [0.61, 1.20] ms, n = 25 neurons/4 mice; p = 0.016, WSR; Figure 5G). Moreover,
350 PTNs in 6-OHDA mice had a progressive increase in AP threshold during repetitive
351 firing (the first AP = -53.7 [-59.1, -50.8] mV, the last AP = -51.1 [-56.6, -44.8] mV, n = 25
352 neurons/4 mice; p = 0.0001, WSR; Figure 5I).

353 When the difference between the first and last APs was analyzed, we found
354 greater differences in the above parameters in PTNs from 6-OHDA mice than those
355 from controls. The AP $width_{(last-first)}$ for controls was 0.006 (-0.004, 0.04) ms, n = 25
356 neurons/5 mice, while for 6-OHDA mice was 0.05 (0.01, 0.10) ms, n = 25 neurons/4
357 mice; p = 0.016, MWU (Figure 5D). The AP decay $rate_{(last-first)}$ for the controls was 2.44 [-

358 3.66, 5.56] mV/ms, n = 25 neurons/5 mice, while the value for 6-OHDA mice was 7.94
359 [4.58, 11.90] mV/ms, n = 25 neurons/4 mice; p = 0.0004, MWU (Figure 5F). The AP
360 decay time$_{(last-first)}$ for controls was -0.015 (-0.045, 0.016) ms, n = 25 neurons/5 mice,
361 while the value for 6-OHDA mice was 0.059 (-0.03, 0.12) ms, n = 25 neurons/4 mice; p
362 = 0.018, MWU (Figure 5H). Finally, the AP threshold$_{(last-first)}$ value for controls was 0.40 [-
363 1.65, 2.78] mV, n = 25 neurons/5 mice, while the value for 6-OHDA mice was 2.96
364 [1.05, 4.07] mV, n = 25 neurons/4 mice; p < 0.006, MWU (Figure 5J). These results
365 suggest that following the loss of midbrain DA neurons the altered intrinsic properties of
366 M1 PTNs impair their capability to sustain constant AP waveforms during repetitive
367 firing, which likely compromises their capacity of fast firing and the temporal precision of
368 motor commands for motor control (Suter et al., 2013; Sauerbrei et al., 2020).
369
370 **Impaired activity of BK channels underlies the decreased intrinsic excitability of**
371 **M1 PTNs following the loss of midbrain DA neurons.**
372 AP width is determined by the time and velocity of depolarization and repolarization
373 (Bean, 2007). Our results above indicated that broadened APs of PTNs following the
374 loss of DA neurons are largely attributed to prolonged AP repolarization. Furthermore,
375 following the loss of midbrain DA neurons, the amplitude of the fast
376 afterhyperpolarization (fAHP) in PTNs diminished (controls = 12.6 [9.8, 14.5] mV, n = 25
377 neurons/5 mice; 6-OHDA = 9.1 [6.0, 12.3] mV, n = 25 neurons/5 mice; p = 0.003, MWU;
378 Figures 6A, B), but the amplitude of median afterhyperpolarization (mAHP) was similar
379 to that of controls (controls = 21.7 [16.6, 24.4] mV, n = 25 neurons/5 mice; 6-OHDA =
380 23.0 [20.1, 26.4] mV, n = 25 neurons/5 mice; p = 0.63, MWU; Figure 6C).

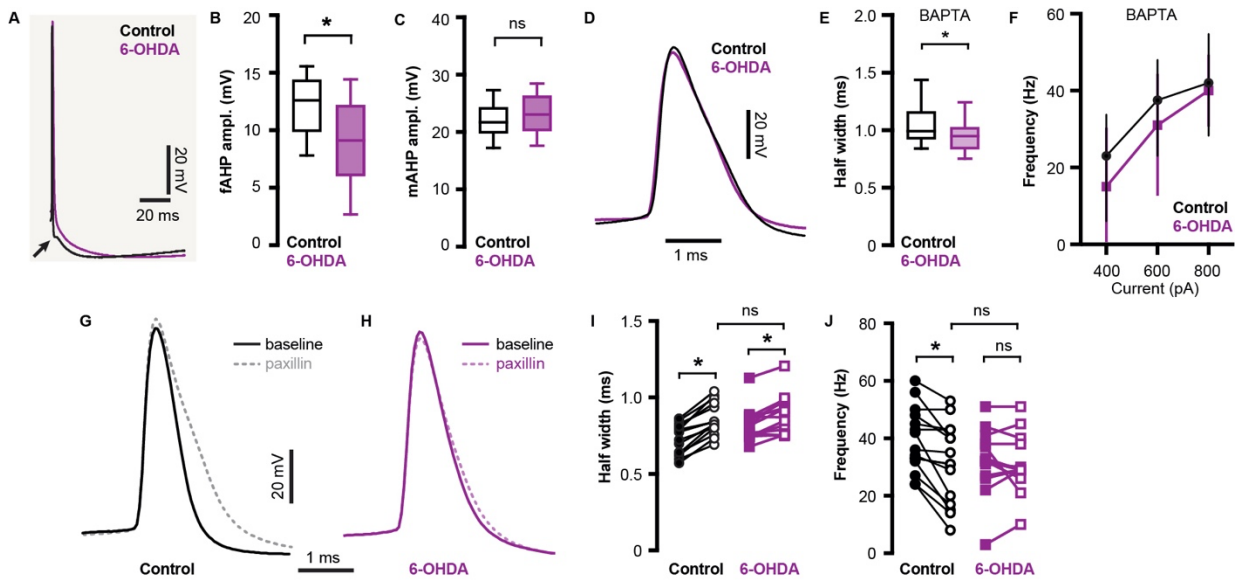

Figure 6. Decreased BK channel activity underlies AP broadening and impaired intrinsic excitability of PTNs following loss of midbrain DA neurons. A) Representative AP waveforms showing diminished fAHPs (arrow) in PTNs from 6-OHDA mice, relative to those from controls. **B-C**) Boxplot showing decreased amplitude of fAHPs (**B**) and unaltered mAHPs (**C**) in PTNs from 6-OHDA mice relative to those from controls. **D**) Representative APs waveforms of PTNs from controls and 6-OHDA mice in the presence of BAPTA. APs were aligned at the threshold and overlaid for comparison. **E**) Boxplot showing reversal of broadened AP of PTNs in 6-OHDA mice relative to controls after intracellular BAPTA dialysis. **F**) Summarized graph showing unaltered excitability of PTNs from 6-OHDA mice relative to those from controls in the presence of BAPTA. The number of APs elicited by 400-, 600-, and 800-pA somatic current injections were compared. **G and H**) Representative APs waveforms before and after paxillin application in PTNs from controls (**G**) and 6-OHDA mice (**H**). APs were aligned at the threshold and overlaid for comparison. **I**) Summarized graph showing paxillin broadened APs of PTNs from both controls and 6-OHDA mice. **J**) Summarized graph showing that paxillin significantly decreased the number of spikes (evoked by injecting 720-pA current) of PTNs from controls but did not affect those from 6-OHDA mice. Application of paxillin occluded the decreased number of spikes of PTNs from 6-OHDA mice relative to those from controls. Filled and open symbols in (**I and J**) indicate the values of before and after paxillin application, respectively. ns, not significant; *, $p < 0.05$, WSR or MWU.

BK currents contribute to fAHPs, AP repolarization and/or AP broadening during repetitive neuronal firing in multiple brain regions (Faber and Sah, 2003; Bean, 2007; Contet et al., 2016). The reduced fAHP amplitude in PTNs from 6-OHDA mice indicates that altered BK channel activity probably underlies broadened AP of PTNs in 6-OHDA mice.

BK channel activation requires both membrane depolarization and Ca^{2+} influx during APs. Therefore, we decreased the activation of BK channels by intracellularly

389 dialyzing a high-affinity Ca^{2+} chelator, BAPTA (10 mM), and determined its effect on the
390 AP width of PTNs from both controls and 6-OHDA mice. In the presence of BAPTA, the
391 AP of PTNs from 6-OHDA mice was slightly and statistically significant narrower (half-
392 width: controls = 0.99 [0.92, 1.17] ms, n = 40 neurons/3 mice; 6-OHDA = 0.95 [0.83,
393 1.03] ms, n = 39 neurons/3 mice; p = 0.029, MWU; Figures 6D, E). In addition, the
394 PTNs from both groups also showed similar intrinsic excitability in the presence of
395 BAPTA (Figure 6F). For example, the number of spikes in response to maximal current
396 injection at 800 pA for controls = 42 [28, 55] spikes, n = 40 neurons/3 mice, while the
397 value for 6-OHDA = 40 [31, 49] spikes, n = 39 neurons/3 mice; p = 0.84, MWU (Figure
398 6F).
399 Furthermore, we blocked BK channels activity by a selective BK channel blocker,
400 paxillin (10 μM), through bath application and we found that it significantly prolonged the
401 APs of PTNs in both groups (Figure 6G, H). The half-width of controls before and after
402 paxillin were 0.77 [0.64, 0.81] ms, and 0.84 [0.8, 0.96] ms, respectively (n = 15
403 neurons/3 mice; p = 0.0001, WSR; Figures 6I). For PTNs from 6-OHDA mice, the half-
404 width before and after paxillin were 0.82 [0.75, 0.87] ms and 0.89 [0.78, 0.98] ms,
405 respectively (n= 14 neurons/3 mice; p = 0.0009, WSR; Figures 6I). With the blockade of
406 BK channels by paxillin, the AP width was not statistically different between PTNs from
407 controls and 6-OHDA mice (MWU, p = 0.62; Figure 6G, I). In addition, paxillin
408 significantly decreased the intrinsic excitability of PTNs from controls (the number of
409 spikes in response to 480-pA current injection, baseline = 36 [32, 48] Hz, paxillin = 31
410 [17, 43] Hz; n = 15 neurons/ 3 mice; p = 0.0002, WSR; Figure 6J). In contrast, paxillin
411 did not affect the number of spikes in PTNs of 6-OHDA mice (spike frequency at 480-pA

current injection, baseline = 32 [27, 39] Hz, paxillin = 29 [28, 39] Hz; n = 14 neurons/ 3 mice; p = 0.71, WSR; Figure 6J). In the presence of paxillin, there is no difference in the intrinsic excitability of PTNs between 6-OHDA mice and controls (MWU, p = 0.7; Figure 6J). Together, these results suggested that impaired BK channel function underlies the broadened APs and decreased intrinsic excitability of PTNs following the loss of midbrain DA neurons.

Intrinsic adaptations of M1 pyramidal neurons were not due to the decreased DA neuromodulation in M1

M1 receives dopaminergic inputs from the ventral tegmental area and these neurons are partially degenerate in 6-OHDA mice (Hosp et al., 2011, 2015; Hosp and Luft, 2013). Thus, we predicted that loss of direct mesocortical DA neuromodulation contributes to the intrinsic adaptations of PTNs and ITNs in M1. To test this prediction, we activated DA receptors on PTNs and ITNs through bath perfusion of DA (10 μM) and determined its impact on the intrinsic properties of M1 PTNs and ITNs from both controls and 6-OHDA mice. The activation of DA receptors by DA produced negligible effects to the intrinsic excitability of M1 PTNs in controls (e.g., the firing frequency at a 360-pA current injection, baseline = 37 [30, 47] Hz; DA = 34 [20, 39] Hz; n = 10 neurons/3 mice; p = 0.25, WSR; Figures. 7A, B). In addition, the application of DA (10 μM) did not produce significant effects to the intrinsic excitability of M1 PTNs in 6-OHDA mice either (e.g., the firing frequency at a 360-pA current injection, baseline = 26 [20, 33] Hz, DA = 27 [19, 36] Hz, n = 14 neurons/3 mice; p = 0.72, WSR; Figures. 7C, D).

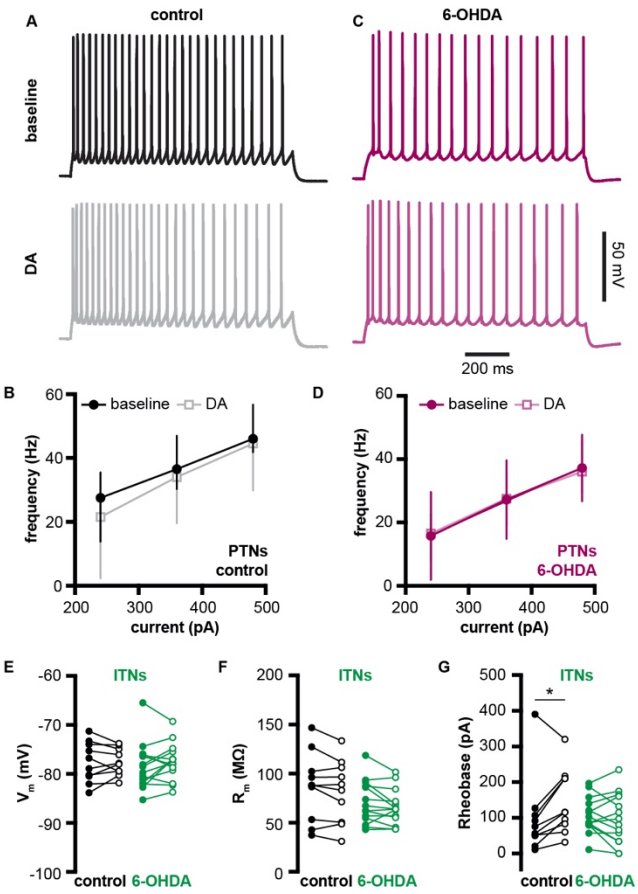

Figure 7. DA application could not rescue intrinsic adaptations in PTNs and ITNs of M1 following loss of midbrain DA neurons. **A-B**) Representative AP traces showing the effect of DA application (10 μM) on the number of APs of PTNs from controls (**A**) and the summarized results (**B**). **C-D**) Representative AP traces showing the effect of DA application on the number of APs of PTNs from 6-OHDA mice (**C**) and the summarized results (**D**). **E-G**) Summarized graphs showing the impact of DA (10 μM) on intrinsic properties of ITNs from controls and 6-OHDA mice, including the V_m (**E**), R_m (**F**), rheobase (**G**) of ITNs from controls and 6-OHDA mice. Filled and open circles in (**E-G**) indicate the values of before and after DA application, respectively Each line connected the rheobase before (filled circle) and after (open circle) DA application. *, $p < 0.05$, WSR.

Furthermore, DA (10 μM) did not alter the AP width of PTNs in both group either (controls: baseline = 0.72 [0.56, 0.8] ms, DA = 0.71 [0.55, 0.84] ms, n = 10 neurons/3 mice, p = 0.32, WSR; 6-OHDA: baseline = 0.74 [0.62, 0.85] ms, 6-OHDA DA = 0.74 [0.57, 0.88] ms, n = 14 neurons/3 mice, p = 0.24, WSR). These data suggested that restoration of local DA neuromodulation cannot rescue the impaired intrinsic excitability and AP broadening of M1 PTNs following the loss of midbrain DA neurons.

Next, we tested whether the altered passive membrane properties of M1 ITNs of 6-OHDA mice (Figure 3) are caused by the loss of local DA neuromodulation. In control mice, the activation of DA receptors by DA (10 μM) did not produce a significant effect on the V_m (baseline = -78 [-81, -74] mV, DA = -78 [-80, -75] mV, n = 10 neurons/2 mice; $p > 0.99$, WSR; Figure 7E) or on the R_m of ITNs (baseline = 88 [51, 109] MΩ, DA = 86

446 [50, 108] MΩ, n = 10 neurons/2 mice; p = 0.16, WSR; Figure 7F). However, the
447 rheobase of ITNs was significantly increased (baseline = 66 [43, 112] pA, DA = 116 [77,
448 212] pA, n = 10 neurons/ 2 mice; p = 0.027, WSR; Figure 7G). On the other hand, in
449 ITNs of 6-OHDA mice, the application of DA (10 μM) did not alter the V_m (baseline = -79
450 [-82, -76] mV, DA = -77 [-80, -75] mV, n = 14 neurons/3 mice; p = 0.22, WSR; Figure
451 7E); the R_m (baseline = 65 [53, 88] MΩ, DA = 64 [53, 75] MΩ, n = 14 neurons/3 mice; p
452 = 0.06, WSR; Figure 7F); or the rheobase (baseline = 95 [80, 145] pA, DA = 90 [34,
453 161] pA, n = 14 neurons/3 mice; p = 0.33, WSR; Figure 7G). Thus, the loss of DA
454 neuromodulation did not play a major role in the cell-type-specific intrinsic adaptations
455 of M1 pyramidal neurons in the parkinsonian state.
456

457 **Discussion**

458 We systematically studied adaptative changes in the intrinsic properties of M1
459 pyramidal neurons in experimental parkinsonism. We found cell-type-specific decrease
460 of the intrinsic excitability PTNs and adaptive changes in the passive membrane
461 properties of ITNs in M1. We also found that prolonged AP repolarization led to AP
462 broadening and resulted in the decreased intrinsic excitability of M1 PTNs. Further, we
463 revealed that impaired BK channel function was the main ionic mechanism underlying
464 the altered AP waveforms and intrinsic excitability of M1 PTNs. Last, we showed that
465 the intrinsic adaptations in M1 PTNs and ITNs were not caused by a loss of
466 mesocortical dopaminergic neuromodulation. Our findings strongly suggest that the loss
467 of midbrain DA neurons not only alters basal ganglia activity, but also triggers intrinsic
468 adaptations in M1 circuitry, which contribute to the reduced motor cortical output and
469 motor deficits in the parkinsonian state.

470 Compelling evidence supports an abnormal rate and pattern of activity in M1 in
471 parkinsonian state, which could be caused by loss of direct mesocortical DA projection,
472 the pathological basal ganglia output associated with nigrostriatal degeneration, or both.
473 (Goldberg et al., 2002; Pasquereau and Turner, 2011; Pasquereau et al., 2016). To
474 distinguish between these possibilities, we employed *ex vivo* electrophysiology to study
475 the intrinsic properties of projection-defined M1 pyramidal neurons. Our findings that
476 PTNs, but not the ITNs, in the L5b of M1 had decreased intrinsic excitability in 6-OHDA
477 mice are consistent with the earlier findings in MPTP-treated primates, showing a cell-
478 type-specific reduction of the firing frequency of M1 pyramidal neurons (Pasquereau
479 and Turner, 2011). Given the innervation of subcortical motor centers by M1 PTNs,

480 these results suggested that intrinsic adaptations of M1 pyramidal neurons contribute to
481 an insufficient motor cortical outputs following the loss of midbrain DA neurons, in
482 addition to an elevated basal ganglia inhibition as proposed by the classical model
483 (Albin et al., 1989; DeLong, 1990; Galvan and Wichmann, 2008). We postulate that
484 these adaptations exacerbate the hypokinetic parkinsonian motor deficits.

485 Distinct changes in the intrinsic excitability of M1 pyramidal neurons cannot be
486 explained by alterations in their passive membrane properties. For example, we found
487 an increased R_m of PTNs in 6-OHDA mice, which might be a homeostatic compensation
488 for, rather than a cause of, their decreased intrinsic excitability. It is possible that the
489 increased R_m makes M1 PTNs more sensitive to and more easily to be entrained by
490 synaptic inputs in the parkinsonian state, including the abnormal basal ganglia signals
491 through the thalamocortical projections. The increased sensitivity of PTNs to synaptic
492 inputs may also disrupts their selectivity in encoding movements. In contrast, ITNs were
493 hyperpolarized and showed a trend of decreased input resistance following the loss of
494 midbrain DA neurons, but these changes were compensated for by other adaptions
495 (e.g., an increased Na_v availability for AP generation), so they did not significantly alter
496 the superathreshold excitability. Together, our data suggested that, intrinsic adaptations
497 play an important role in the cell-type-specific alterations of the activity of M1 pyramidal
498 neurons following the loss of midbrain DA neurons. The molecular mechanisms
499 underlying cell-type specific adaptations in M1 in parkinsonian state should be
500 determined in future studies.

501 APs of PTNs were significantly broadened following the loss of DA neurons and it
502 was largely due to a prolonged repolarization (Figures 4A-E). AP width has significant

503 impact on Ca^{2+} influx during APs, which further controls the quantity and kinetics of
504 neurotransmitter release and synaptic plasticity at axon terminal (Bean, 2007). Thus, we
505 suggest that AP broadening is a compensatory mechanism for the decreased intrinsic
506 excitability of M1 PTNs in parkinsonian state in order to maintain stable motor cortical
507 outputs, though this possibility should be further studied. We further showed that the AP
508 broadening in PTNs from 6-OHDA mice was occluded in the presence of BAPTA and
509 paxillin, indicating a key role of BK channels in the intrinsic adaptations of M1 PTNs in
510 parkinsonian state (Shao et al., 1999; Faber and Sah, 2003; Bean, 2007). Indeed, it has
511 been proposed that impaired function or inactivation of BK channels that underlies AP
512 repolarization and/or fAHPs could slow the de-inactivation of Na_v channels during AP
513 and reduce Na_v availability for the subsequent AP generation, leading to a decreased
514 excitability (Bean, 2007; Jaffe et al., 2011). A progressive and accumulative Na_v
515 inactivation is consisted with our observations that PTNs in 6-OHDA mice showed
516 stronger spike adaptation during repetitive firing relative to those from controls
517 (Fleidervish et al., 1996), though the contribution of the other mechanisms such as the
518 M-current can't be discounted (Buchta et al., 2017; Parrilla-Carrero et al., 2018). It is
519 intriguing that in the presence of BAPTA PTNs from 6-OHDA mice exhibited narrower
520 APs than those from controls (Figures 6D, E). It indicates the involvement of other ionic
521 mechanisms in controlling of AP repolarizationof PTNs, e.g., K_v conductance (e.g., K_v3
522 and K_v4) (Rudy and McBain, 2001; Pathak et al., 2016; Soares et al., 2017).
523 An acute application of DA did not rescue altered intrinsic excitability of PTNs
524 and had minimal effects to intrinsic properties of ITNs in 6-OHDA mice. This indicated
525 that loss of dopaminergic neuromodulation does not play a major role in the intrinsic

526 adaptations of M1 pyramidal neurons in parkinsonian state, which is consistent with
527 recent findings that dopaminergic modulation of pyramidal neurons is mainly mediated
528 indirectly by parvalbumin-expressing interneurons in M1 (Vitrac et al., 2014; Cousineau
529 et al., 2020). Thus, we propose that circuitry mechanisms underlie cellular adaptions in
530 M1 in parkinsonian state. For example, recent work highlighted the critical role indirect
531 pathway SPN hyperactivity in driving cellular and synaptic adaptations in basal ganglia
532 nuclei, such as the subthalamic nucleus (Chu et al., 2017; Sharott et al., 2017; Ryan et
533 al., 2018; McIver et al., 2019). Thus, it is likely that the pathological basal ganglia
534 outputs following loss of DA that drive adaptive changes in the intrinsic properties of M1
535 pyramidal neurons, which are mediated by thalamocortical projections.

536 The exaggerated rhythmic activity and aberrant oscillations in the basal ganglia
537 circuitry are closely related to the expression of motor symptoms in PD (Bevan et al.,
538 2002; Little and Brown, 2014; Hemptinne et al., 2015). Indeed, the motor cortex exhibits
539 abnormal neural activity in parkinsonian state at both the single-cell and population
540 levels (Goldberg et al., 2002; Pasquereau and Turner, 2011; Hemptinne et al., 2015;
541 Pasquereau et al., 2016). Moreover, both experimental and computation studies have
542 indicated that cerebral cortical inputs play a crucial role in orchestrating pathological
543 activity in basal ganglia nuclei (e.g., the external global pallidus and the subthalamic
544 nucleus) (Bevan et al., 2002; Magill et al., 2004; Kita and Kita, 2011; Corbit et al., 2016;
545 Chu et al., 2017; Sharott et al., 2017). Recent studies further showed that electrical or
546 optogenetic stimulation of the motor cortical pyramidal neurons and/or their projections
547 produced therapeutic effects in parkinsonian animals (Gradinaru et al., 2009; Li et al.,
548 2012; Hemptinne et al., 2015; Sanders and Jaeger, 2016; Magno et al., 2019). Thus, an

549 in-depth understanding of motor cortical adaptations in PD at the cellular and circuitry

550 levels will help to design better therapeutic approaches with fewer off-target effects.

551

552 **Figure legends**

553 **Figure 1**. **Decreased intrinsic excitability of PTNs in the L5b of M1 following the**
554 **loss of midbrain DA neurons. A and B**) Representative graphs showing the injection
555 site of red Retrobeads in the pontine nuclei (**A**) and a retrogradely labeled PTN in L5b of
556 M1 (**B**). **C and D**) Representative spike trains of PTNs evoked by somatic current
557 injections from controls and 6-OHDA mice (**C**), and the frequency-current relationship of
558 the PTNs from controls and 6-OHDA mice (**D**). **E-G**) Boxplots showing a reduced gain
559 of spike-current curve (**E**), a decreased firing frequency in response to maximal current
560 injections (i.e., 720 pA) (**F**), and an enhanced spike adaptations (**G**) in PTNs from 6-
561 OHDA mice relative to those from controls. *, $p < 0.05$, MWU.

562

563 **Figure 2. Intact intrinsic excitability of ITNs in the M1 L5b following the loss of**
564 **midbrain DA neurons. A and B**) Representative graphs showing the injection site of
565 green Retrobeads in the dorsal striatum (**A**) and retrogradely labeled ITNs (**B**). **C and**
566 **D)** Representative spikes trains evoked by somatic current injections into ITNs from
567 control and 6-OHDA mice (**C**), and the frequency-current relationship of ITNs from
568 controls and 6-OHDA mice (**D**). **E-G**) Boxplots showing an unaltered gain of spike-
569 current curve (**E**), firing frequency in response to maximal current injections (i.e., 720
570 pA) (**F**), and spike adaptation (**G**) between ITNs from 6-OHDA mice and controls. ns,
571 not significant, MWU.

572

573 **Figure 3**. **Distinct changes in the passive membrane properties of PTNs and ITNs**
574 **in the M1 L5b following loss of midbrain DA neurons**. **A-C**) Boxplots showing

575 changes in the resting membrane potential (**A**), input resistance (**B**), and rheobase (**C**)
576 of PTNs from 6-OHDA mice relative to those from controls. **D-F**) Boxplots showing
577 changes in in the resting membrane potential (**D**), input resistance (**E**), and rheobase
578 (**F**) of ITNs from 6-OHDA mice relative to those from controls. ns, not significant; *, $p <$
579 0.05, MWU.
580
581 **Figure 4. Distinct changes in AP waveforms of PTNs and ITNs in the M1 L5b**
582 **following loss of midbrain DA neurons. A**) **Top**, representative AP waveforms of
583 PTNs from controls and 6-OHDA mice. APs were aligned at threshold and overlaid for
584 comparison. **Bottom**, the corresponding *d*V/*d*t traces plotted against time, showing
585 depolarizing and repolarizing rates of APs. **B**) Boxplot showing broadened AP width in
586 PTNs from 6-OHDA mice relative to those from controls. **C and D**), Boxplots showing
587 prolonged AP rise time (**C**) and decay time (**D**) in PTNs from 6-OHDA mice relative to
588 those from controls. **E and F**), Boxplots showing decreased AP rise rate (**E**) and decay
589 rate (**F**) in PTNs from 6-OHDA mice relative to those from controls. **G**) **Top**,
590 representative AP waveforms of ITNs from controls and 6-OHDA mice. APs were
591 aligned at threshold and overlaid for comparison. **Bottom**, the corresponding *d*V/*d*t
592 traces plotted against time, showing depolarizing and repolarizing rates of APs. **H**)
593 Boxplot showing similar AP width in ITNs from 6-OHDA mice relative to those from
594 controls. **I-J**) Boxplots showing a shorter AP rise time (**I**) but similar decay time (**J**) in
595 ITNs from 6-OHDA mice relative to those from controls. **K-L**) Boxplots showing an
596 increased AP rise rate (**K**) but similar decay rate (**L**) in ITNs from 6-OHDA mice relative
597 to those from controls. ns, not significant; *, $p < 0.05$, MWU.

598 **Figure 5**. **Progressive changes in AP waveforms of M1 PTNs during repetitive**
599 **firing. A-B**) APs from a 10- to15-Hz spike train were superimposed for PTN from
600 control (**A**) or 6-OHDA mice (**B**). APs were aligned at threshold, and the solid and
601 dashed lines indicated the first and the last APs from the spike train, respectively. All the
602 other APs were shown as transparent lines. **C-D**) Summarized graphs showing the
603 alterations of AP width between the first and the last APs. Each line in (**C**) connects the
604 AP width of the first and the last APs from the same spike train. Filled and open circles
605 indicate the median plus interquartile range of the first and the last AP width of PTNs,
606 respectively. (**D**) Boxplots showing the difference between the AP width of the first and
607 the last APs was greater in PTNs from 6-OHDA mice relative to those from controls. **E-**
608 **F**) Summarized graphs showing alterations of AP decay rate between the first and the
609 last APs (**E**) and greater changes of AP decay rate in PTNs from 6-OHDA mice relative
610 to those from controls (**F**). **G-H**) Summarized graphs showing alterations of AP decay
611 time between the first and the last APs (**G**), and greater changes of AP decay time in
612 PTNs from 6-OHDA mice relative to those from controls (**H**). **I-J**) Summarized graphs
613 showing alterations of AP threshold between the first and the last APs (**I**), and greater
614 changes of AP threshold in PTNs from 6-OHDA mice relative to those from controls (**J**).
615 ns, not significant; *, $p < 0.05$, WSR.
616
617 **Figure 6. Decreased BK channel activity underlies AP broadening and impaired**
618 **intrinsic excitability of PTNs following loss of midbrain DA neurons. A**)
619 Representative AP waveforms showing diminished fAHPs (arrow) in PTNs from 6-OHDA
620 mice, relative to those from controls. **B-C**) Boxplot showing decreased amplitude of fAHPs

621 (**B**) and unaltered mAHPs (**C**) in PTNs from 6-OHDA mice relative to those from controls.
622 **D**) Representative APs waveforms of PTNs from controls and 6-OHDA mice in the
623 presence of BAPTA. APs were aligned at the threshold and overlaid for comparison. **E**)
624 Boxplot showing reversal of broadened AP of PTNs in 6-OHDA mice relative to controls
625 after intracellular BAPTA dialysis. **F**) Summarized graph showing unaltered excitability of
626 PTNs from 6-OHDA mice relative to those from controls in the presence of BAPTA. The
627 number of APs elicited by 400-, 600-, and 800-pA somatic current injections were
628 compared. **G and H**) Representative APs waveforms before and after paxillin application
629 in PTNs from controls (**G**) and 6-OHDA mice (**H**). APs were aligned at the threshold and
630 overlaid for comparison. **I**) Summarized graph showing paxillin broadened APs of PTNs
631 from both controls and 6-OHDA mice. **J**) Summarized graph showing that paxillin
632 significantly decreased the number of spikes (evoked by injecting 720-pA current) of
633 PTNs from controls but did not affect those from 6-OHDA mice. Application of paxillin
634 occluded the decreased number of spikes of PTNs from 6-OHDA mice relative to those
635 from controls. Filled and open symbols in (**I and J**) indicate the values of before and after
636 paxillin application, respectively. ns, not significant; *, $p < 0.05$, WSR or MWU.
637
638 **Figure 7**. DA application could not rescue intrinsic adaptations in PTNs and ITNs of M1
639 following loss of midbrain DA neurons. **A-B**) Representative AP traces showing the
640 effect of DA application (10 μM) on the number of APs of PTNs from controls (**A**) and
641 the summarized results (**B**). **C-D**) Representative AP traces showing the effect of DA
642 application on the number of APs of PTNs from 6-OHDA mice (**C**) and the summarized
643 results (**D**). **E-G**) Summarized graphs showing the effect of DA (10 μM) on intrinsic

644 properties of ITNs from controls and 6-OHDA mice, including the V_m (**E**), R_m (**F**),
645 rheobase (**G**) of ITNs from controls and 6-OHDA mice. Filled and open circles in (**E-G**)
646 indicate the values of before and after DA application, respectively. Each line connected
647 the rheobase before (filled circle) and after (open circle) DA application. *, $p < 0.05$,
648 WSR.
649
650
651
652
653
654
655
656

References cited:

Albin RL, Young AB, Penney JB (1989) The functional anatomy of basal ganglia disorders. Trends Neurosci 12:366–375.

Barthas F, Kwan AC (2017) Secondary motor cortex: where ‘sensory’ meets ‘motor’ in the rodent frontal cortex. Trends Neurosci 40:181–193.

Bean BP (2007) The action potential in mammalian central neurons. Nat Rev Neurosci 8:451–465.

Bevan MD, Magill PJ, Terman D, Bolam JP, Wilson CJ (2002) Move to the rhythm: oscillations in the subthalamic nucleus–external globus pallidus network. Trends Neurosci 25:525–531.

Bodor ÁL, Giber K, Rovó Z, Ulbert I, Acsády L (2008) Structural correlates of efficient GABAergic transmission in the basal ganglia–thalamus pathway. J Neurosci 28:3090–3102.

Buchta WC, Mahler SV, Harlan B, Aston-Jones GS, Riegel AC (2017) Dopamine terminals from the ventral tegmental area gate intrinsic inhibition in the prefrontal cortex. Physiol Rep 5:e13198.

Chu H-Y, Atherton JF, Wokosin D, Surmeier DJ, Bevan MD (2015) Heterosynaptic regulation of external globus pallidus inputs to the subthalamic nucleus by the motor cortex. Neuron 85:364–376.

676 Chu H-Y, McIver EL, Kovaleski RF, Atherton JF, Bevan MD (2017) Loss of hyperdirect
677 pathway cortico-subthalamic inputs following degeneration of midbrain dopamine
678 neurons. Neuron 95:1306-1318.e5.

679 Contet C, Goulding SP, Kuljis DA, Barth AL (2016) BK channels in the central nervous
680 system. Int Rev Neurobiol 128:281–342.

681 Corbit VL, Whalen TC, Zitelli KT, Crilly SY, Rubin JE, Gittis AH (2016) Pallidostriatal
682 projections promote β oscillations in a dopamine-depleted biophysical network model. J
683 Neurosci 36:5556–5571.

684 Cousineau J, Lescouzères L, Taupignon A, Delgado-Zabalza L, Valjent E, Baufreton J,
685 Bon-Jégo ML (2020) Dopamine D2-like receptors modulate intrinsic properties and
686 synaptic transmission of parvalbumin interneurons in the mouse primary motor cortex.
687 Eneuro:ENEURO.0081-20.2020.

688 DeLong MR (1990) Primate models of movement disorders of basal ganglia origin.
689 Trends Neurosci 13:281–285.

690 Ebbesen CL, Brecht M (2017) Motor cortex — to act or not to act? Nat Rev Neurosci
691 18:694–705.

692 Ebbesen CL, Doron G, Lenschow C, Brecht M (2017) Vibrissa motor cortex activity
693 suppresses contralateral whisking behavior. Nat Neurosci 20:82–89.

694 Ebbesen CL, Insanally MN, Kopec CD, Murakami M, Saiki A, Erlich JC (2018) More
695 than just a “motor”: recent surprises from the frontal cortex. J Neurosci 38:9402–9413.

696 Economo MN, Viswanathan S, Tasic B, Bas E, Winnubst J, Menon V, Graybuck LT,
697 Nguyen TN, Smith KA, Yao Z, Wang L, Gerfen CR, Chandrashekar J, Zeng H, Looger
698 LL, Svoboda K (2018) Distinct descending motor cortex pathways and their roles in
699 movement. Nature 563:79–84.

700 Faber ESL, Sah P (2003) Ca2+-activated K+ (BK) channel inactivation contributes to
701 spike broadening during repetitive firing in the rat lateral amygdala. J Physiol 552:483–
702 497.

703 Fieblinger T, Graves SM, Sebel LE, Alcacer C, Plotkin JL, Gertler TS, Chan CS,
704 Heiman M, Greengard P, Cenci MA, Surmeier DJ (2014) Cell type-specific plasticity of
705 striatal projection neurons in parkinsonism and L-DOPA-induced dyskinesia. Nat
706 Commun 5:5316.

707 Fleidervish IA, Friedman A, Gutnick MJ (1996) Slow inactivation of Na+ current and
708 slow cumulative spike adaptation in mouse and guinea-pig neocortical neurones in
709 slices. J Physiol 493:83–97.

710 Galvan A, Wichmann T (2008) Pathophysiology of parkinsonism. Clin Neurophysiology
711 Official J Int Fed Clin Neurophysiology 119:1459–1474.

712 Gittis AH, Hang GB, LaDow ES, Shoenfeld LR, Atallah BV, Finkbeiner S, Kreitzer AC
713 (2011) Rapid target-specific remodeling of fast–spiking inhibitory circuits after loss of
714 dopamine. Neuron 71:858–868.

715 Goldberg JA, Boraud T, Maraton S, Haber SN, Vaadia E, Bergman H (2002) Enhanced
716 synchrony among primary motor cortex neurons in the 1-Methyl-4-Phenyl-1,2,3,6-
717 Tetrahydropyridine primate model of Parkinson's disease. J Neurosci 22:4639–4653.

718 Gradinaru V, Mogri M, Thompson KR, Henderson JM, Deisseroth K (2009) Optical
719 deconstruction of parkinsonian neural circuitry. Science 324:354–359.

720 Guo J-Z, Graves AR, Guo WW, Zheng J, Lee A, Rodríguez-González J, Li N, Macklin
721 JJ, Phillips JW, Mensh BD, Branson K, Hantman AW (2015a) Cortex commands the
722 performance of skilled movement. Elife 4:e10774.

723 Guo L, Xiong H, Kim J-I, Wu Y-W, Lalchandani RR, Cui Y, Shu Y, Xu T, Ding JB
724 (2015b) Dynamic rewiring of neural circuits in the motor cortex in mouse models of
725 Parkinson's disease. Nat Neurosci 18:1299–1309.

726 Hemptinne C de, Swann NC, Ostrem JL, Ryapolova-Webb ES, Luciano MS,
727 Galifianakis NB, Starr PA (2015) Therapeutic deep brain stimulation reduces cortical
728 phase-amplitude coupling in Parkinson's disease. Nat Neurosci 18:779–786.

729 Hosp JA, Luft AR (2013) Dopaminergic meso-cortical projections to M1: role in motor
730 learning and motor cortex plasticity. Front Neurol 4:145.

731 Hosp JA, Nolan HE, Luft AR (2015) Topography and collateralization of dopaminergic
732 projections to primary motor cortex in rats. Exp Brain Res 233:1365–1375.

733 Hosp JA, Pekanovic A, Rioult-Pedotti MS, Luft AR (2011) Dopaminergic projections
734 from midbrain to primary motor cortex mediate motor skill learning. J Neurosci 31:2481–
735 2487.

736 Jaffe DB, Wang B, Brenner R (2011) Shaping of action potentials by type I and type II
737 large-conductance Ca2+-activated K+ channels. Neuroscience 192:205–218.

738 Kawai R, Markman T, Poddar R, Ko R, Fantana AL, Dhawale AK, Kampff AR, Ölveczky
739 BP (2015) Motor cortex is required for learning but not for executing a motor skill.
740 Neuron 86:800–812.

741 Kita H, Kita T (2011) Cortical stimulation evokes abnormal responses in the dopamine-
742 depleted rat basal ganglia. J Neurosci 31:10311–10322.

743 Kress GJ, Yamawaki N, Wokosin DL, Wickersham IR, Shepherd GMG, Surmeier DJ
744 (2013) Convergent cortical innervation of striatal projection neurons. Nat Neurosci
745 16:665–667.

746 Lee J, Wang W, Sabatini BL (2020) Anatomically segregated basal ganglia pathways
747 allow parallel behavioral modulation. Nat Neurosci. In press.

748 Li Q, Ke Y, Chan DCW, Qian Z-M, Yung KKL, Ko H, Arbuthnott GW, Yung W-H (2012)
749 Therapeutic deep brain stimulation in parkinsonian rats directly influences motor cortex.
750 Neuron 76:1030–1041.

751 Little S, Brown P (2014) The functional role of beta oscillations in Parkinson's disease.
752 Parkinsonism Relat D 20 Suppl 1:S44-8.

753 Magill PJ, Sharott A, Bevan MD, Brown P, Bolam JP (2004) Synchronous unit activity
754 and local field potentials evoked in the subthalamic nucleus by cortical stimulation. J
755 Neurophysiol 92:700–714.

756 Magno LAV, Tenza-Ferrer H, Collodetti M, Aguiar MFG, Rodrigues APC, Silva RS da,
757 Silva J do P, Nicolau NF, Rosa DVF, Birbrair A, Miranda DM, Romano-Silva MA (2019)
758 Optogenetic stimulation of the M2 cortex reverts motor dysfunction in a mouse model of
759 Parkinson's disease. J Neurosci 39:3234–3248.

760 Mallet N, Pogosyan A, Sharott A, Csicsvari J, Bolam JP, Brown P, Magill PJ (2008)
761 Disrupted dopamine transmission and the emergence of exaggerated beta oscillations
762 in subthalamic nucleus and cerebral cortex. J Neurosci 28:4795–4806.

763 Mathai A, Ma Y, Paré J-F, Villalba RM, Wichmann T, Smith Y (2015) Reduced cortical
764 innervation of the subthalamic nucleus in MPTP-treated parkinsonian monkeys. Brain
765 138:946–962.

766 McGregor MM, Nelson AB (2019) Circuit mechanisms of Parkinson's disease. Neuron
767 101:1042–1056.

768 McIver EL, Atherton JF, Chu H-Y, Cosgrove KE, Kondapalli J, Wokosin D, Surmeier DJ,
769 Bevan MD (2019) Maladaptive downregulation of autonomous subthalamic nucleus
770 activity following the loss of midbrain dopamine neurons. Cell Reports 28:992-1002.e4.

771 Oswald MJ, Tantirigama MLS, Sonntag I, Hughes SM, Empson RM (2013) Diversity of
772 layer 5 projection neurons in the mouse motor cortex. Front Cell Neurosci 7:174.

773 Parker JG, Marshall JD, Ahanonu B, Wu Y-W, Kim TH, Grewe BF, Zhang Y, Li JZ, Ding
774 JB, Ehlers MD, Schnitzer MJ (2018) Diametric neural ensemble dynamics in
775 parkinsonian and dyskinetic states. Nature 557:177–182.

776 Parker PRL, Lalive AL, Kreitzer AC (2016) Pathway-specific remodeling of
777 thalamostriatal synapses in parkinsonian mice. Neuron 89:734–740.

778 Parrilla-Carrero J, Buchta WC, Goswamee P, Culver O, McKendrick G, Harlan B,
779 Moutal A, Penrod R, Lauer A, Ramakrishnan V, Khanna R, Kalivas P, Riegel AC (2018)
780 Restoration of Kv7 channel-mediated inhibition reduces cued-reinstatement of cocaine
781 seeking. J Neurosci 38:4212–4229.

782 Pasquereau B, DeLong MR, Turner RS (2016) Primary motor cortex of the parkinsonian
783 monkey: altered encoding of active movement. Brain 139:127–143.

784 Pasquereau B, Turner RS (2011) Primary motor cortex of the parkinsonian monkey:
785 differential effects on the spontaneous activity of pyramidal tract-type neurons. Cereb
786 Cortex 21:1362–1378.

787 Pathak D, Guan D, Foehring RC (2016) Roles of specific Kv channel types in
788 repolarization of the action potential in genetically identified subclasses of pyramidal
789 neurons in mouse neocortex. J Neurophysiol 115:2317–2329.

790 Rudy B, McBain CJ (2001) Kv3 channels: voltage-gated K+ channels designed for high-
791 frequency repetitive firing. Trends Neurosci 24:517–526.

792 Ryan MB, Bair-Marshall C, Nelson AB (2018) Aberrant striatal activity in parkinsonism
793 and levodopa-induced dyskinesia. Cell Reports 23:3438-3446.e5.

794 Sanders TH, Jaeger D (2016) Optogenetic stimulation of cortico-subthalamic projections
795 is sufficient to ameliorate bradykinesia in 6-OHDA lesioned mice. Neurobiol Dis 95:225–
796 237.

797 Sauerbrei BA, Guo J-Z, Cohen JD, Mischiati M, Guo W, Kabra M, Verma N, Mensh B,
798 Branson K, Hantman AW (2020) Cortical pattern generation during dexterous
799 movement is input-driven. Nature 577:386–391.

800 Shao L, Halvorsrud R, Borg-Graham L, Storm JF (1999) The role of BK-type Ca2+-
801 dependent K+ channels in spike broadening during repetitive firing in rat hippocampal
802 pyramidal cells. J Physiol 521:135–146.

803 Sharott A, Vinciati F, Nakamura KC, Magill PJ (2017) A population of indirect pathway
804 striatal projection neurons is selectively entrained to parkinsonian beta oscillations. J
805 Neurosci 37:9977–9998.

806 Sheets PL, Suter BA, Kiritani T, Chan CS, Surmeier DJ, Shepherd GMG (2011)
807 Corticospinal-specific HCN expression in mouse motor cortex: Ih -dependent synaptic
808 integration as a candidate microcircuit mechanism involved in motor control. J
809 Neurophysiol 106:2216–2231.

810 Shen W, Plotkin JL, Francardo V, Ko WKD, Xie Z, Li Q, Fieblinger T, Wess J, Neubig
811 RR, Lindsley CW, Conn PJ, Greengard P, Bezard E, Cenci MA, Surmeier DJ (2015) M4

812 muscarinic receptor signaling ameliorates striatal plasticity deficits in models of L-
813 DOPA-induced dyskinesia. Neuron 88:762–773.

814 Shepherd GMG (2013) Corticostriatal connectivity and its role in disease. Nat Rev
815 Neurosci 14:278–291.

816 Shimamoto SA, Ryapolova-Webb ES, Ostrem JL, Galifianakis NB, Miller KJ, Starr PA
817 (2013) Subthalamic nucleus neurons are synchronized to primary motor cortex local
818 field potentials in Parkinson's disease. J Neurosci 33:7220–7233.

819 Soares D, Goldrick I, Lemon RN, Kraskov A, Greensmith L, Kalmar B (2017)
820 Expression of Kv3.1b potassium channel is widespread in macaque motor cortex
821 pyramidal cells: A histological comparison between rat and macaque. J Comp Neurol
822 525:2164–2174.

823 Sreenivasan V, Esmaeili V, Kiritani T, Galan K, Crochet S, Petersen CCH (2016)
824 Movement initiation signals in mouse whisker motor cortex. Neuron 92:1368–1382.

825 Suter BA, Migliore M, Shepherd GMG (2013) Intrinsic electrophysiology of mouse
826 corticospinal neurons: a class-specific triad of spike-related properties. Cereb Cortex
827 23:1965–1977.

828 Viaro R, Morari M, Franchi G (2011) Progressive motor cortex functional reorganization
829 following 6-hydroxydopamine lesioning in rats. J Neurosci 31:4544–4554.

830 Vila M, Périer C, Féger J, Yelnik J, Faucheux B, Ruberg M, Raisman-Vozari R, Agid Y,
831 Hirsch EC (2000) Evolution of changes in neuronal activity in the subthalamic nucleus of

832 rats with unilateral lesion of the substantia nigra assessed by metabolic and
833 electrophysiological measurements. Eur J Neurosci 12:337–344.

834 Villalobos C, Shakkottai VG, Chandy KG, Michelhaugh SK, Andrade R (2004) SKCa
835 channels mediate the medium but not the slow calcium-activated afterhyperpolarization
836 in cortical neurons. J Neurosci 24:3537–3542.

837 Vitrac C, Péron S, Frappé I, Fernagut P-O, Jaber M, Gaillard A, Benoit-Marand M
838 (2014) Dopamine control of pyramidal neuron activity in the primary motor cortex via D2
839 receptors. Front Neural Circuit 8:13.

840 Wang X, Liu Y, Li X, Zhang Z, Yang H, Zhang Y, Williams PR, Alwahab NSA, Kapur K,
841 Yu B, Zhang Y, Chen M, Ding H, Gerfen CR, Wang KH, He Z (2017) Deconstruction of
842 corticospinal circuits for goal-directed motor skills. Cell 171:440-455.e14.

843 Willard AM, Isett BR, Whalen TC, Mastro KJ, Ki CS, Mao X, Gittis AH (2019) State
844 transitions in the substantia nigra reticulata predict the onset of motor deficits in models
845 of progressive dopamine depletion in mice. Elife 8:e42746.

846